An Inter-Doppler Interference Constrained OC-DFE for OTFS in UWA Communications

Yang Yang, *Student Member, IEEE,* Lu Ma, *Member, IEEE,* Boon-Chong Seet, *Senior Member, IEEE,*

***Abstract*—Orthogonal Time Frequency Space (OTFS) modulation presents a promising approach for underwater acoustic (UWA) communication. This study proposes an iterative decision feedback equalizer based on optimal combining (OC) for UWA-OTFS systems, addressing challenges posed by the full-matrix channel characteristics in the delay-Doppler domain. The proposed detector maximizes the signal-to-interference-plus-noise ratio of the combined signal. Furthermore, by introducing inter-Doppler interference depth, the OC detector dynamically constrains the number of combining terms. Simulation results demonstrate that the proposed detector effectively balances bit error rate performance with computational complexity.**

***Index Terms*—UWA, OTFS, detector, Doppler factor, DFE, adaptive, OC, interference correlation**

I. INTRODUCTION

UNDERWATER acoustic (UWA) communication plays a pivotal role in marine information exchange [1]. Orthogonal time-frequency space (OTFS) communication technology is widely considered an effective solution to the high-reliability communication in high-speed mobile scenarios [2]. In the field of UWA communication, OTFS detection has attracted widespread interest for research, including linear minimum mean squared error (LMMSE) detectors [3], [4], various deep learning-based detectors such as convolutional neural networks and deep neural networks [5]–[7], and the unitary approximate message passing nonlinear detection method [8]. As highlighted by a survey on OTFS detectors [9], nonlinear detectors often require higher complexity to achieve a better performance. In comparison, the iterative decision feedback equalizer based on maximal ratio combining (MRC-DFE) detection method proposed in [10], which relies on a deterministic model, achieves a fine balance between design complexity and performance.

Unlike radio communication, UWA multicarrier systems constitute wideband transmissions that are highly susceptible to severe inter-Doppler interference (IDI) in UWA channels. These effects contribute to double spreading in the delay-Doppler (DD) domain [11], [12], which causes the DD domain channel matrix to exhibit full-matrix characteristics. The received components of transmitted symbols in the DD domain are not only related to the actual channel delay branches, but also to the adjacent delay branches of the actual multipath components [3]. As the Doppler spread rises, there is an increase in the number of received multipath components of the transmitted symbols, which leads to a higher complexity for the MRC-DFE scheme. On the other hand, in the presence of correlated interference, optimal combining (OC) demonstrates significant advantages over MRC in linear diversity combining schemes [13], [14].

To address significant IDI in UWA channels, this paper proposes an IDI-constrained OC-DFE, inspired by the work of [10]. The remainder of this paper is organized as follows. Section II outlines the UWA-OTFS communication system model, while Section III elaborates on the design of proposed equalizer. In Section IV the simulation results are discussed. Section V presents the conclusion.

Notation: Vectors, matrices, and scalars are denoted by $\mathbf{x}$, $\mathbf{X}$, and x, respectively. The notations $\mathbf{X}^T$, $\mathbf{X}^\dagger$ and $\mathbf{X}^*$ denote the transpose, Hermitian transpose and complex conjugate, respectively. The matrices $\mathbf{I}_N$, $\mathbf{F}_N$, and $\mathbf{F}_N^\dagger$ represent the N-dimensional identity matrix, the N-point discrete Fourier transform (DFT) matrix, and the N-point inverse discrete Fourier transform (IDFT) matrix, respectively. The Kronecker product is denoted by $\otimes$, and $vec\{\mathbf{X}\}$ represents the vector obtained by stacking the columns of the matrix $\mathbf{X}$. The operation $vec_{N\times M}^{-1}(\mathbf{a})$ converts a vector $\mathbf{a}$ into an $N \times M$ matrix by arranging it column-wise. The column vectors $\mathbf{x}_m$ and $\mathbf{y}_m$ represent the mth row of the matrices $\mathbf{X}$ and $\mathbf{Y}$, where m (row) represents the delay index, and n (column) represents the Doppler index. The number of elements in a set Ω is denoted by $|\Omega|$. We denote $\|\mathbf{x}\|_2^2$ and $\|\mathbf{X}\|_F^2$ as the squared 2-norm of vector $\mathbf{x}$ and the squared Frobenius norm of matrix $\mathbf{X}$, respectively.

II. SYSTEM MODEL

Let $\mathbf{X}$ represent the transmitted two-dimensional DD grid, which contains a frame of $M \times N$ $\mathcal{Q}$-QAM symbols. The matrix $\mathbf{X}_{dt}$ represents the delay-time (DT) domain sampling matrix. By applying the rectangular window $\mathbf{I}_M \in \mathbb{C}^{M\times M}$, the matrix $\mathbf{X}_{dt}$ is vectorized to obtain the signal vector $\mathbf{s} \in \mathbb{C}^{NM\times 1}$, which is transmitted over the physical channel. Through the inverse discrete Zak transform [15], the relation-

This research was supported in part by the National Key Research and Development Program of China under Grant 2023YFC3010800, in part by the National Natural Science Foundation of China under Grant 62271161, in part by the Key Research and Development Program of Shandong Province under Grant 2022CXGC020409, and in part by the National Key Laboratory of Underwater Acoustic Technology under Grant 2023-JCJQ-LB-072-08. The work of Yang Yang was supported by the Chinese Scholarship Council (CSC).

Yang Yang and Lu Ma is with the National Key Laboratory of Underwater Acoustic Technology, the Key Laboratory of Marine Information Acquisition and Security (Ministry of Industry and Information Technology), and the College of Underwater Acoustic Engineering, Harbin Engineering University, Harbin 150001, China, Lu Ma is also with Sanya Nanhai Innovation and Development Base of Harbin Engineering University, Sanya 572024, China (e-mail: heu_yangyang@hotmail.com, malu@hrbeu.edu.cn).

Boon-Chong Seet is with the Department of Electrical and Electronic Engineering, Auckland University of Technology, Auckland 1010, New Zealand. (e-mail: boon-chong.seet@aut.ac.nz).

ship between the time-domain sampled signal $\mathbf{s}$ and the DD domain symbol $\mathbf{X}$ is expressed as

$$\mathbf{s} = vec(\mathbf{I}_M \cdot \mathbf{X} \cdot \mathbf{F}_N^{\dagger}). \tag{1}$$

Subsequent to up-conversion, a passband continuous-time signal is obtained as $\tilde{s}(t) = s(t)e^{j2\pi f_c t}$. With the passband signal sent to the underwater physical channel, UWA channel modeling [16] is expressed as

$$h(t) = \sum_{p=1}^{P} h_p \delta((1+\alpha_p)t - \tau_p) \tag{2}$$

where, h_p, α_p, and τ_p represent the amplitude gain, Doppler factor, and delay of the pth path, respectively. The relationship between the Doppler factor α_p and the relative velocity v_p is expressed as $\alpha_p = v_p/c$, where c refers to the sound speed. Then, the passband received signal is resampled with the estimated Doppler factor $\hat{\alpha}$ to obtain

$$\tilde{y}_r(t) = \sum_{p=1}^{P} h_p \tilde{s}((1+b_p)(t-\tau'_p)) + \tilde{n}(t/(1+\hat{\alpha})) \tag{3}$$

where $b_p = \frac{1+\alpha_p}{1+\hat{\alpha}} - 1$ is the residual Doppler factor, and the effective delay expansion is $\tau'_p = \frac{\tau_p}{1+b_p}$. The advantage of this approach is that resampling eliminates the average Doppler factors across all paths, which leads to a residual Doppler factor with a mean value of 0 [17].

Following down-conversion, the baseband received signal is obtained as $y(t) = \tilde{y}_r(t)e^{-j2\pi f_c t}$. Accordingly, baseband sampled signal is expressed $y[i'] = y(i'/B)$. The discrete time series $i' = 0, 1, ..., L-1, L = [MN + B\tau_{\max}]$ is defined as the maximum number of samples of the delay scale channel output signal. Matrixing

$$\mathbf{r} = \mathbf{G} \cdot \mathbf{s} + \bar{\mathbf{n}} \tag{4}$$

$\mathbf{G} \in \mathbb{C}^{L \times MN}$ represents the time domain baseband equivalent channel matrix. At the receiver, a rectangular window shaping filter $\mathbf{I}_M$ is also employed. In this case, the discrete time domain sampling signal $\mathbf{r} \in \mathbb{C}^{MN \times 1}$ is matrixed by column to obtain the DT domain sampling signal $\mathbf{Y}_{dt} = vec_{N,M}^{-1}(\mathbf{r})$. Through discrete Zak transform, the DD domain sampling matrix $\mathbf{Y}$ is obtained

$$\mathbf{Y}^T = \mathbf{F}_N {\mathbf{Y}_{dt}}^T \tag{5}$$

where $\mathbf{Y} \in \mathbb{C}^{M \times N}$ represents the received two-dimensional DD grid. The matrix is vectorized to further explore the characteristics of the equivalent channel matrix in the DD domain. The input-output relationship of the UWA-OTFS system in the DD domain can be expressed as

$$\mathbf{y} = \mathbf{H} \cdot \mathbf{x} + \mathbf{n} \tag{6}$$

where, $\mathbf{x}, \mathbf{y}, \mathbf{n} \in \mathbb{C}^{MN \times 1}$, $\mathbf{H} \in \mathbb{C}^{NM \times NM}$ represent OTFS transmit symbols, receive symbols, noise vector and DD domain equivalent channel matrix, respectively.

Thus, the delay scale channel matrix $\mathbf{G}$ can be related to the DD domain matrix $\mathbf{H}$ as

$$\mathbf{H} = \mathbf{P}^T \cdot (\mathbf{F}_N \otimes \mathbf{I}_M) \cdot \mathbf{G} \cdot \left(\mathbf{F}_N^{\dagger} \otimes \mathbf{I}_M\right) \cdot \mathbf{P} \tag{7}$$

where, matrix $\mathbf{P}$ is a row-column interleaver permutation matrix that rearranges elements of the input vector according to specific rules to achieve a *perfect shuffle* [10]. According to [10], the channel matrix $\mathbf{H}$ is reconstructed using the block matrix $\mathbf{K}_{m,q} \in \mathbb{C}^{N \times N}, q = 0 : M-1$. Due to the spectral leakage caused by the $\mathrm{sinc}(\cdot)$ function, the equivalent channel exhibits spreading in the branches adjacent to the true channel delay positions. IDI manifests as interference between adjacent delay branches, propagating to the D delay branches directly neighboring each true channel delay tap [18]. D is defined as the IDI-depth corresponding to each real channel delay branch. Since the residual Doppler factor is small enough, the channel matrix shows band sparsity. The approximated band sparsity matrix is defined as $\mathbf{H}_D$.

The block matrix $\mathbf{K}_{m,q}^D$ in the approximate matrix $\mathbf{H}_D$ under the IDI-depth D constraint is expressed as

$$\mathbf{K}_{m,q}^D = \begin{cases} \mathbf{K}_{m,q}, & q \in \Omega \\ 0, & else \end{cases} \tag{8}$$

$\mathbf{K}_{m,q}^D$ can be considered as the linear time variant channel between the receiver grid delay index m and transmitter grid delay index $m-q$ in the DD grid. The set $\Omega = \{l \pm D : l \in \ell\}$ represents the delay branches with significant contributions from the DD domain transmission symbol component, and ℓ refers to the set of discrete delay indices l of the true channel. It is worth noting that the elements in the set Ω are unique.

III. IDI-Constrained OC-DFE Algorithm

In this section, we propose an IDI-constrained OC-DFE , which dynamically constrains IDI-depth during iterative detection to maximize signal-to-interference-plus-noise ratio (SINR) while reducing complexity in UWA-OTFS systems.

A. Optimal combining considering interference correlation

The input-output relationship between the transmitted symbol vector $\mathbf{x}_m$ and the received symbol vector $\mathbf{y}_m$ can be reformulated as

$$\mathbf{y}_{m+q} = \sum_{q \in \Omega} \mathbf{K}_{m+q,q}^D \cdot \mathbf{x}_m + \mathbf{w}_{m+q}. \tag{9}$$

Considering the sparsity of the channel matrix blocks, it is assumed that the transmitted symbol $\mathbf{x}_m$ contributes signal components to $Q\,(|\ell| < Q = |\Omega| < M)$ received symbol vectors $\mathbf{y}_{m+q}$. $\mathbf{b}_m^q \in \mathbb{C}^{N \times 1}$ is defined as the channel-impaired signal component of $\mathbf{x}_m$ in the received vector $\mathbf{y}_{m+q}$ at the delay index $m+q$, after eliminating the interference caused by other transmitted symbol vectors $\mathbf{x}_k$ for $k \neq m$. The component $\mathbf{b}_m^q$ can be expressed as

$$\mathbf{b}_m^q = \mathbf{y}_{m+q} - \sum_{q' \in \Omega, q' \neq q} \mathbf{K}_{m+q,q'}^D \cdot \hat{\mathbf{x}}_{m+q-q'} \tag{10}$$

where, the signal component of $\mathbf{b}_m^q$ is expressed as $\mathbf{a}_{m,q} = \mathbf{K}_{m+q,q}^D \cdot \hat{\mathbf{x}}_m$, while the non-signal component $\mathbf{n}_{m,q}$ is comprised of noise $\mathbf{w}_{m+q}$ plus interference terms. The interference term primarily emerges from three key sources: (i) approximation errors inherent in the banded sparse channel matrix constrained by the IDI-depth parameter D as depicted in (8),

which constitute the primary correlation source of channel interference. (ii) Channel estimation inaccuracies and (iii) symbol estimation errors accumulated in preceding iterative processes, with the interference from these two components gradually diminishing as the number of iterations increases. The non-signal component is expressed as

$$\mathbf{n}_{m,q} = \mathbf{y}_{m+q} - \sum_{q\in\Omega} \mathbf{K}^{D}_{m+q,q} \cdot \hat{\mathbf{x}}_m. \tag{11}$$

Unlike wireless channels [10], the impaired signal components $\mathbf{b}_m^q$ corresponding to each delay element remain susceptible to significant interference and noise, which leads to the relatively poor performance of MRC. In the presence of strong interference and noise, performing OC from the perspective of maximizing SINR can achieve considerable reception gains [13], [14], [19]. Therefore, the implementation of OC will be discussed under the following assumptions:

- The symbols $\hat{\mathbf{x}}_m$ to be estimated are derived from the modulation alphabet with equal probability distribution, with its average power normalized to 1.

- The non-signal vectors $\mathbf{n}_{m,q}, q = 1, \cdots, Q-1$, are independently and identically distributed (i.i.d.), complex Gaussian, with $E[\mathbf{n}_{m,q}] = 0$ and the covariance is σ^2.

$\mathbf{W} = [\mathbf{W}_1, ..., \mathbf{W}_j, ..., \mathbf{W}_J]^T \in \mathbb{C}^{NJ\times N}$ is defined as the OC coefficient matrix that maximizes the SINR for each delay branch. $\mathbf{W}_j \in \mathbb{C}^{N\times N}$, as the submatrix of $\mathbf{W}$, represents the weighting component corresponding to the impaired signal component $\mathbf{b}_m^q$ of the jth delay branch. The index j represents the position of the element q in the set Ω under the IDI-depth constraint, sorted in ascending order relative to the entire set, i.e., $j = \mathrm{rank}_\Omega(q)$. The total number of delay branches contributing to the current decision symbol is $J = Q = |\Omega|$. The SINR after combining is denoted as μ

$$\mu = \left\| \sum\nolimits_{j=1}^{J} \mathbf{W}_j \mathbf{K}_{m,q} \right\|_F^2 \Big/ \left\| \sum\nolimits_{j=1}^{J} \mathbf{W}_j \mathbf{n}_{m,q} \right\|_F^2. \tag{12}$$

The maximum SINR (12) is obtained

$$\max_{\mathbf{W}} \left(Tr\left[\left(\mathbf{W}^T\mathbf{K}\right) \left(\mathbf{W}^T\mathbf{K}\right)^\dagger \right] \Big/ Tr\left[\mathbf{W}^T \left(\mathbf{R}\otimes\mathbf{I}_N\right) \mathbf{W}^* \right] \right) \tag{13}$$

$\mathbf{K} = [\mathbf{K}^D_{m,1}, \mathbf{K}^D_{m,2}, \ldots, \mathbf{K}^D_{m,J}]^T \in \mathbb{C}^{NJ\times N}$ is composed of submatrices $\mathbf{K}^D_{m,q}$. The elements of the covariance matrix of the non-signal components in the mth delay branch, denoted as $\mathbf{R} \in \mathbb{C}^{J\times J}$

$$R(j_1, j_2) = E\left[\frac{\mathbf{n}_{m,j_2} \cdot \mathbf{n}^\dagger_{m,j_1}}{\|\mathbf{n}_{m,j_1}\| \, \|\mathbf{n}_{m,j_2}\|} \right] \tag{14}$$

where $R(j_1, j_2)$ represents the normalized inner product of the j_1th and j_2th sub-vectors of the vector $\mathbf{n}$, indicating the level of correlation between the two column vectors. $\mathbf{R}\otimes\mathbf{I}_N$ represents a positive definite Hermitian matrix, which can be decomposed as

$$\mathbf{R}\otimes\mathbf{I}_N = \mathbf{P}^H \mathbf{\Lambda}^2 \mathbf{P}. \tag{15}$$

The unitary matrix $\mathbf{P}$ is established by the eigenvectors associated with the eigenvalues of the $\mathbf{R}\otimes\mathbf{I}_N$. $\mathbf{\Lambda}^2$ represents a real-valued $NJ \times NJ$ diagonal matrix, with the diagonal elements corresponding to the eigenvalues of $\mathbf{R}\otimes\mathbf{I}_N$. The trace operation is expressed as the square of the norm

$$\max_{\mathbf{W}} \left(\left\| (\mathbf{\Lambda}\mathbf{P}\mathbf{W}^*)^\dagger (\mathbf{\Lambda}^{-1}\mathbf{P}\mathbf{K}) \right\|_F^2 \Big/ \left\| (\mathbf{\Lambda}\mathbf{P}\mathbf{W}^*) \right\|_F^2 \right). \tag{16}$$

The Frobenius norm of a matrix product satisfies the property of submultiplicativity, with Holder's inequality used for matrix traces. When the equality holds, the optimal combining coefficient $\mathbf{W}$ for the Q delay branches is

$$\mathbf{W} = \mathbf{R}^{-1} \otimes \mathbf{I}_N \cdot \mathbf{K}^*. \tag{17}$$

Specifically, when the interference plus noise components of the delay branches are mutually independent, OC is equivalent to MRC, i.e. $\mathbf{W} = \mathbf{K}^*$.

B. IDI-constrained OC-DFE algorithm

The proposed IDI-constrained OC-DFE dynamically selects $Q = |\Omega|$ signal components based on the current channel conditions. The process is detailed in Algorithm 1.

Algorithm 1 IDI-constrained OC-DFE algorithm.

Require: $\mathbf{H}, \mathbf{K}, \mathbf{y}_m, \mathbf{x}_m = \mathbf{x}^{(0)}, D = 0, \varepsilon$
for $D = 0 : M' - 1$ **do**
  Compute $\bar{\gamma}^D_{SIR}$ through (18)
  if $\left|\bar{\gamma}^D_{SIR} - \bar{\gamma}^{D-1}_{SIR}\right| \le \varepsilon$ **then**
    break
  end if
end for
for $i = 1$: maxiterations **do**
  for $m = 0 : M-1$ **do**
    for $q \in \Omega$ **do**
      Calculate $\mathbf{b}_m^{q(i)}$ and $\mathbf{n}^{(i)}_{m,q}$ as in (10) and (11)
    end for
    Update $\mathbf{R}^{(i)}$, $\mathbf{c}^{(i)}_m$ and $\mu^{(i)}_m$ as in (14), (19) and (12)
    $\hat{\mathbf{x}}^{(i)}_m = sgn\left(\mathbf{c}^{(i)}_m\right)$
  end for
  if $mean(\mathbf{u}^{(i)}) < 1$ **then**
    $D = D + 1$
  end if
end for
Ensure: $\hat{\mathbf{x}}_m$

Firstly, the channel matrix is reconstructed from the estimated channel parameters employing the embedded pilot structure [20]. Under the current channel conditions, D is updated flexibly by evaluating the signal-to-IDI ratio (SIR), as the result of which the initial number of delay branches to be combined can be determined. Similar to the signal-to-ICI ratio definition [21], the SIR indicates the interference level of the actual channel delay branches $\{l, l \in \ell\}$ caused by the adjacent temporal branches within the IDI

$$\bar{\gamma}^D_{SIR} = \mathop{\mathrm{E}}_{0\le m\le M-1} \left[\frac{\sum_{q:q\in Q} \|\mathbf{K}_{m,q}\|_F^2}{\sum_{q:q\notin Q} \|\mathbf{K}_{m,q}\|_F^2} \right]. \tag{18}$$

When the ith iteration, the channel-impaired signal components $(\mathbf{b}_m^q)^{(i)}$ and the non-signal components $\mathbf{n}^{(i)}_{m,q}$ are calculated firstly according to (10) and (11), utilizing the symbol

vector $\hat{\mathbf{x}}_m^{(i-1)}$ from the previous iteration. The covariance matrix $\mathbf{R}^{(i)}$ is computed using (14), the OC output vector $\mathbf{c}_m^{(i)}$ is obtained

$$\mathbf{c}_m^{(i)} = \mathbf{D}_m^{-1} \cdot \sum_{j=1}^{J} \mathbf{W}_j \cdot \left(\mathbf{b}_m^j\right)^{(i)} \tag{19}$$

where

$$\mathbf{W} = \left(\mathbf{R}^{-1}\right)^{(i)} \otimes \mathbf{I}_N \cdot \mathbf{K}^* \tag{20}$$

$$\mathbf{D}_m = \sum_{q \in \Omega} \mathbf{K}^{\dagger}_{m+q,q} \cdot \mathbf{K}_{m+q,q}. \tag{21}$$

To ensure numerical stability in computing the OC weight $\mathbf{W}$, a regularization term is incorporated to stabilize the inversion of the interference covariance matrix $\mathbf{R}$. After hard decision, the symbol vector $\hat{\mathbf{x}}_m^{(i)}$ is obtained as follows

$$\hat{x}_m^{(i)}(n) = \arg\min \left| g_a - c_m^{(i)}(n) \right| \tag{22}$$

where, g_a represents a signal from the $\mathcal{Q}$-QAM symbols, $n = 0, \ldots, N-1$. The operator $sgn(\cdot)$ denotes the decision function applied to the estimated symbol vector $\mathbf{c}_m$ during each iteration. Hard-decision is given by the maximum likelihood (ML) criterion in (22). A soft-decision approach employing probabilistic thresholds, as comprehensively described in [22], may also be adopted.

With the symbol vector estimated for each delay index, the SINR value μ corresponding to the current iteration is calculated. Finally, the SINR vector $\mathbf{u}$ corresponding to the M delay symbols is obtained, and its average value is computed. A smaller the average value than 1, indicates that the interference energy exceeds the signal energy. In this case, the next iteration is performed with an increment of 1 in IDI-depth D. In most cases, initial value of IDI-depth D is sufficient to achieve satisfactory equalization performance.

The computational complexity of Algorithm 1 is analyzed in terms of multiplication operations. After determining parameter D, the number of combining terms in each iteration is fixed. The complexity of obtaining $\bar{\gamma}_{SIR}^{D}$ is $\mathcal{O}(2M'QN^2)$. In the m-th iteration, extracting $\mathbf{b}_m^q$ and $\mathbf{n}_{m,q}$ requires $\mathcal{O}(2N^2Q(Q-1))$, while computing the correlation matrix $\mathbf{R}$ costs $\mathcal{O}(3NQ^2)$. The OC process to obtain $\mathbf{c}_m$ requires $\mathcal{O}(QN^3 + N^3 + Q(N^2 + QN^3))$, and checking the convergence condition needs $\mathcal{O}(QN^3 + N^2 + QN^2 + N)$. Given the maximum iteration number I, the overall complexity of Algorithm 1 is $\mathcal{O}\left(IMN\left(2NQ^2 + 3Q^3 + 2QN^2 + N^2 + Q^2N^2\right)\right)$, $Q \ll M$. Compared to the MRC scheme, the OC scheme requires additional computation of the non-signal component $\mathbf{n}_{m,q}$ and its corresponding correlation matrix $\mathbf{R}$, introducing an extra computational overhead of $\mathcal{O}\left(3NQ^2 + 2N^2Q(Q-1)\right)$ per iteration. The OC detector requires storage capacity of $(Q+1)MN$ complex numbers, comprising QMN delay channel coefficients and M symbol vector estimates during each iteration.

IV. SIMULATION RESULTS

A UWA-OTFS system with a center frequency of 7 kHz and a bandwidth of 4 kHz is considered. The number of symbols in the Doppler domain and delay domain are denoted as $N = 64$ and $M = 64$, respectively. Under are 4-QAM modulation scheme, a zero-padded guard interval occupies half of the total delay symbols, i.e., $M_{ZP} = M/2$. The corresponding communication rate is 4 kbps, with a spectral efficiency of 1 bps/Hz. As a result, when the maximum delay spread of the channel is within 8 ms, the cyclic property of the channel matrix block is ensured.

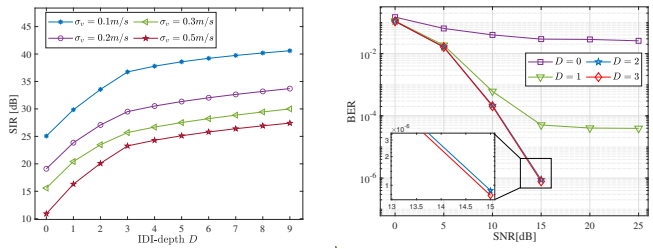

Fig. 1. (a) SIR versus IDI-depth D. (b) IDIC-OC-DFE equalizer performance at varying D.

To evaluate the performance, a random UWA multipath channel is used [17], [18], [23], [24]. The settings are details as follow: The time intervals between two consecutive paths are exponentially distributed with an average value of 2 ms. The amplitudes of the paths conform to Rayleigh distribution, with their average power decreasing exponentially as the delay is extended. Uniformly distributed within $[-1\times10^{-3}, 1\times10^{-3}]$, the Doppler factors exhibit a standard deviation of σ_v m/s. The average Doppler factor $\hat{\alpha}$, estimated by maximizing the cross-correlation with a prepended linear frequency modulated (LFM) preamble, is utilized for resampling to effectuate initial Doppler compensation.

Fig. 1(a) shows the normalized SIR versus IDI-depth for different σ_v. Indicating that the stronger the time-varying nature of the channel, the larger the required IDI-depth. Moreover, as the IDI-depth continues to increase, the growth of SIR slows down and gradually stabilizes. At this point, there are no more significant advantages created by considering more delay branches.

Fig. 1(b) illustrates the bit error rate (BER) performance of the IDI-Constrained OC-DFE (IDIC-OC-DFE) scheme at different depths D when the path velocity standard deviation is $\sigma_v = 0.2$ m/s. Once D is determined by the proposed equalizer, the number of combined items is also fixed. When $D = 0$, the selected delay branches correspond to the real channel, thus resulting in the unsatisfactory equalization performance. As the depth D gradually increases, the BER performance ceases to show improvement with the rising D. At this point, the optimal selection of depth D is achieved. It is also implied that the precise recovery of information bits is achievable with limited complexity when the IDI-depth is accurately selected.

Fig. 2(a) shows the BER performance of the IDIC-OC-DFE at varying σ_v. When $\sigma_v = 0.5$, the BER ceases to decrease with increase in SNR, with the BER approaching 10^{-4}. It is also indicated that the proposed equalizer is supposed to satisfy the assumption that the channel matrix is band sparse. When $\sigma_v = 0.1$ and $\sigma_v = 0.2$, the BER curves

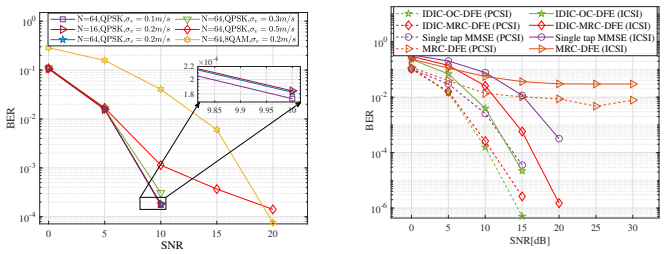

(a) (b)

Fig. 2. (a) IDIC-OC-DFE equalizer perfomance with $M = 64$.
(b) BER performance of different equalizers.

are basically identical, which demonstrates that the IDIC-OC-DFE is robust to Doppler effects due to the adaptive selection of delay branches. Furthermore, comparisons involving different modulation orders (8QAM) and frame sizes (N=16) demonstrate the ability of the adaptive IDI depth mechanism to accommodate diverse system parameters without the need for scenario-specific readjustment.

Fig. 2(b) compares the BER performance of different equalizers under both perfect and imperfect channel state information (PCSI and ICSI, respectively) conditions when $\sigma_v = 0.2$ m/s. Consistent with the performance verification methods for existing data detectors [10], [11], [17], [23], [25], this paper assumes that PCSI is available. The ICSI is obtained by superimposing a Gaussian random matrix on the PCSI channel matrix [26]. Since the MRC-DFE ignores IDI caused by residual Doppler, its performance is significantly worse, which suggests that considering IDI renders channel equalization clearly advantageous. Under ICSI conditions, channel estimation errors cause the SINR after OC to fall below the theoretical optimum, thereby degrading detection performance. However, the estimated covariance matrix can still capture the variations in interference characteristics, thereby enabling OC to better accommodate these errors compared to the MRC method.

V. CONCLUSION

In this paper, a linear complexity equalizer suitable for UWA-OTFS was proposed. The impact of residual Doppler factors was considered after resampling and IDI-depth was introduced to measure the interference. Additionally, an OC detector was proposed to maximize the SINR, with the number of combined terms determined flexibly. Simulation results demonstrated that the proposed scheme achieved superior performance and exhibited robustness to channel estimation errors.

REFERENCES

[1] D. Sun, J. Wu, X. Hong, C. Liu, H. Cui, and B. Si, "Iterative double-differential direct-sequence spread spectrum reception in underwater acoustic channel with time-varying Doppler shifts," *J. Acoust. Soc. Amer.*, vol. 153, no. 2, pp. 1027–1041, 2023.

[2] P. Raviteja, K. T. Phan, Y. Hong, and E. Viterbo, "Interference cancellation and iterative detection for orthogonal time frequency space modulation," *IEEE Trans. Wireless Commun.*, vol. 17, no. 10, pp. 6501–6515, 2018.

[3] X. Wang, X. Shi, J. Wang, and Z. Sun, "Iterative LMMSE-SIC Detector for DSE-Aware Underwater Acoustic OTFS Systems," *IEEE Trans. Veh. Technol.*, 2024.

[4] Q. Wang, N. Zhao, L. Jing, C. He, and C. Zhou, "A Low Complexity Turbo MMSE Equalization Method for OTFS Underwater Acoustic Communications," in *Proc. IEEE Int. Conf. Signal Process., Commun. Comput.* . IEEE, 2023, pp. 1–5.

[5] S. Zhang, Y. Zhang, J. Chang, B. Wang, and W. Bai, "DNN-based signal detection for underwater OTFS systems," in *Proc. IEEE/CIC Int. Conf. Commun. China*. IEEE, 2022, pp. 348–352.

[6] Y. Zhang, S. Zhang, B. Wang, Y. Liu, W. Bai, and X. Shen, "Deep Learning-Based Signal Detection for Underwater Acoustic OTFS Communication," *J. Mar. Sci. Eng.*, vol. 10, no. 12, p. 1920, 2022.

[7] Y. Li, B. Wang, G. Shao, S. Shao, and X. Pei, "Blind detection of underwater acoustic communication signals based on deep learning," *IEEE Access*, vol. 8, pp. 204 114–204 131, 2020.

[8] Z. Xue, Q. Wang, L. Jing, C. Zhou, and C. He, "Unitary approximate message passing detection method for OTFS underwater acoustic communication system," in *Proc. IEEE Int. Conf. Signal Process., Commun. Comput. (ICSPCC)*. IEEE, 2023, pp. 1–5.

[9] M. Aldababsa, S. Özyurt, G. K. Kurt, and O. Kucur, "A survey on orthogonal time frequency space modulation," *IEEE Open J. Commun. Soc.*, 2024.

[10] T. Thaj and E. Viterbo, "Low complexity iterative rake decision feedback equalizer for zero-padded OTFS systems," *IEEE Trans. Veh. Technol.*, vol. 69, no. 12, pp. 15 606–15 622, 2020.

[11] K. Arunkumar and C. R. Murthy, "Orthogonal delay scale space modulation: A new technique for wideband time-varying channels," *IEEE Trans. Signal Process.*, vol. 70, pp. 2625–2638, 2022.

[12] S. Liu, H. Yan, L. Ma, Y. Liu, and X. Han, "UACC-GAN: A Stochastic Channel Simulator for Underwater Acoustic Communication," *IEEE J. Ocean. Eng.*, vol. 49, no. 4, pp. 1605–1621, 2024.

[13] J. P. Burke, J. R. Zeidler, and B. D. Rao, "CINR difference analysis of optimal combining versus maximal ratio combining," *IEEE Trans. Wireless Commun.*, vol. 4, no. 1, pp. 1–5, 2005.

[14] A. Shah and A. M. Haimovich, "Performance analysis of optimum combining in wireless communications with Rayleigh fading and cochannel interference," *IEEE Trans. Commun.*, vol. 46, no. 4, pp. 473–479, 1998.

[15] Z. Wei, S. Li, W. Yuan, R. Schober, and G. Caire, "Orthogonal time frequency space modulation—Part I: fundamentals and challenges ahead," *IEEE Commun. Lett.*, vol. 27, no. 1, pp. 4–8, 2023.

[16] S. Zhou and Z. Wang, *OFDM for underwater acoustic communications*. John Wiley & Sons, 2014.

[17] B. Li, S. Zhou, M. Stojanovic, L. Freitag, and P. Willett, "Multicarrier communication over underwater acoustic channels with nonuniform Doppler shifts," *IEEE J. Ocean. Eng.*, vol. 33, no. 2, pp. 198–209, 2008.

[18] C. R. Berger, S. Zhou, J. C. Preisig, and P. Willett, "Sparse channel estimation for multicarrier underwater acoustic communication: From subspace methods to compressed sensing," *IEEE transactions on signal processing*, vol. 58, no. 3, pp. 1708–1721, 2009.

[19] G. Wu, G. Qiao, L. Ma, and Z. Sun, "A pre-detected combiner under spatial correlated noise in deep ocean of underwater acoustic communication system," *Appl. Acoust.*, vol. 223, p. 110092, 2024.

[20] P. Raviteja, K. T. Phan, and Y. Hong, "Embedded pilot-aided channel estimation for OTFS in delay–Doppler channels," *IEEE Trans. Veh. Technol.*, vol. 68, no. 5, pp. 4906–4917, 2019.

[21] Q. Lu, Y. Huang, Z. Wang, and S. Zhou, "Characterization and receiver design for underwater acoustic channels with large Doppler spread," in *Proc. IEEE/MIT OCEANS Conf.*, 2015, pp. 1–6.

[22] T. Thaj and E. Viterbo, "Low-complexity linear diversity-combining detector for MIMO-OTFS," *IEEE wireless communications letters*, vol. 11, no. 2, pp. 288–292, 2021.

[23] J. Huang, S. Zhou, J. Huang, C. R. Berger, and P. Willett, "Progressive inter-carrier interference equalization for OFDM transmission over time-varying underwater acoustic channels," *IEEE J. Sel. Top. Signal Process.*, vol. 5, no. 8, pp. 1524–1536, 2011.

[24] L. Wan, H. Jia, F. Zhou, M. Muzzammil, T. Li, and Y. Huang, "Fine Doppler scale estimations for an underwater acoustic CP-OFDM system," *Signal Processing*, vol. 170, p. 107439, 2020.

[25] Z. A. Qasem, J. Wang, H. A. Leftah, H. Sun, S. Hong, J. Qi, and H. Esmaiel, "Real signal DHT-OFDM with index modulation for underwater acoustic communication," *IEEE J. Ocean. Eng.*, vol. 48, no. 1, pp. 246–259, 2022.

[26] H. Zhang, X. Huang, and J. A. Zhang, "Adaptive transmission with frequency-domain precoding and linear equalization over fast fading channels," *IEEE Trans. Wireless Commun.*, vol. 20, no. 11, pp. 7420–7430, 2021.